

Reliability-based Design Optimization of Nonlinear Energy Sinks

Ethan Boroson¹ and Samy Missoum²

¹ University of Arizona, Tucson, USA, ethanboroson@email.arizona.edu

² University of Arizona, Tucson, USA, smissoum@email.arizona.edu

1. Abstract

Nonlinear Energy Sinks (NESs) are a promising technique for passively reducing the amplitude of vibrations, especially for use as energy pumping devices for buildings under seismic loading. Through nonlinear stiffness properties, a NES is able to passively and irreversibly absorb energy. Unlike the traditional Tuned Mass Damper (TMD), the NES has no inherent natural frequency, allowing the NES to absorb energy over a wide range of frequencies. The efficiency of the NES, however, is extremely sensitive to small perturbations in design parameters or initial conditions. In many cases, it has been observed that the most efficient NES designs are in fact very close to low efficiency regions in the design space.

This work will present an optimization technique for NESs. In order to optimize NES devices, the high sensitivity of NES to uncertainty, with almost discontinuous behaviors, requires specific reliability-based design optimization (RBDO) techniques. In this work, a support vector machine classifier, insensitive to discontinuities, is used to construct the boundaries of the failure domain (low efficiency regions) through adaptive sampling and clustering. Several RBDO results for various NES configurations will be provided. In particular, NES configurations in parallel will be investigated.

2. Keywords: Nonlinear Energy Sinks, RBDO, SVM, Clustering.

3. Introduction

Nonlinear Energy Sinks (NESs) are an emerging technique for passive and irreversible reduction of amplitude of vibration [3]. NESs have a wide variety of applications, such as energy pumping away from a building under seismic loading [8, 9] or in aeroelasticity [4]. NESs rely on a nonlinear, typically cubic, stiffness property which is at the origin of the irreversible transfer of energy. Two NES configurations are typically used in the literature: Configuration I—NES coupled to a vibrating system through a weak linear spring, and connected to the ground via a nonlinear spring—and Configuration II—NES with small mass directly coupled to linear system through nonlinear spring [7]. The effectiveness of a NES with small mass makes the configuration II NES ideal for use in a building under seismic loading [9].

NESs are often proposed as an alternative to Tuned Mass Dampers (TMDs) that are widely used to absorb and dissipate energy from a vibrating main system. NESs act passively, like TMDs, but unlike TMDs, they do not have to be tuned to a specific natural frequency to effectively dissipate energy from the vibrating main system. Instead, NESs absorb energy over a wide range of natural frequencies, which is particularly attractive in designing a system with a changing natural frequency.

It has been observed that NESs are very sensitive to perturbations in design parameters or loading conditions, leading to a near discontinuous behavior of performance metrics such as the amount of absorbed energy. This discontinuous behavior allows one to identify two distinct regions: one where energy pumping occurs and another one where it does not [7, 2].

4. Configuration II NES

The Configuration II NES consists of a small mass directly coupled to a linear system through a nonlinear spring. A simple two DOF system can be used to illustrate the principles of NES behavior and is depicted in figure 1a. It is composed of a main system 1 (with angular eigen-frequency ω_1 , damping λ_1) and a sub-system 2 (the NES) with nonlinear stiffness α , damping λ_2 and mass ratio (NES mass divided by main system mass) ϵ . The system is excited through an initial velocity (\dot{x}_0) applied to the main system. The full system behavior is calculated through equation 1. The efficiency of the NES is quantified by the percentage of initial energy that the NES dissipates ($E_{NES_{inf}}$), expressed in equation 2 [7].

$$\begin{cases} \ddot{x} + \lambda_1 \dot{x} + \lambda_2 (\dot{x} - \dot{y}) + \omega_1^2 x + \alpha (x - y)^3 = 0 \\ \epsilon \ddot{y} + \lambda_2 (\dot{y} - \dot{x}) + \alpha (y - x)^3 = 0 \end{cases} \quad (1)$$

$$E_{NES_{inf}} = \lim_{t \rightarrow \infty} \frac{\lambda_2 \int_0^t (\dot{y}(\tau) - \dot{x}(\tau))^2 d\tau}{\frac{1}{2} v_1^2} \quad (2)$$

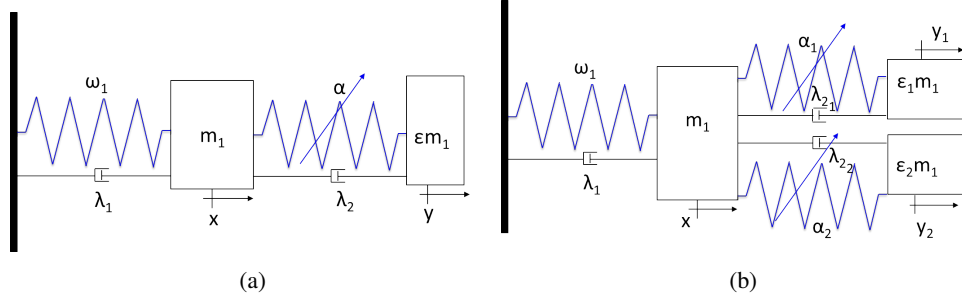


Figure 1: One (a) and Two (b) Configuration II NES systems

This article also details a 3 DOF case where two NESs in parallel are coupled to a main system as in figure 1b. The equations of motion in this case are given in equation 3 [6]. The efficiency of the two NES system is measured as the combined percentage of energy dissipated by the two NESs.

$$\begin{cases} \ddot{x} + \lambda_1 \dot{x} + \lambda_{21}(\dot{x} - \dot{y}_1) + \lambda_{22}(\dot{x} - \dot{y}_2) + \omega_1^2 x + \alpha_1(x - y_1)^3 + \alpha_2(x - y_2)^3 = 0 \\ \varepsilon_1 \ddot{y}_1 + \lambda_{21}(\dot{y}_1 - \dot{x}) + \alpha_1(y_1 - x)^3 = 0 \\ \varepsilon_2 \ddot{y}_2 + \lambda_{22}(\dot{y}_2 - \dot{x}) + \alpha_2(y_2 - x)^3 = 0 \end{cases} \quad (3)$$

5. Discontinuities and activation thresholds

The sensitivity of the efficiency of the NES to small perturbations can be very marked [7], [2]. Figure 2a provides an example where $E_{NES_{inf}}$ is plotted as a function of \dot{x}_0 . A discontinuity occurs at $\dot{x}_0 = 0.15$ m/s, but there is also a relatively steep decay of $E_{NES_{inf}}$ as \dot{x}_0 is further increased. These jumps can be seen as activation energy necessary for energy pumping to occur [6]. At the threshold of the activation energy, the NES performance will be extremely efficient, but beyond the threshold the performance deteriorates. Each NES has a relatively narrow range of initial energies where energy dissipation is high. Similar marked changes in behavior appear when studying $E_{NES_{inf}}$ as a function of design parameters α and ε (figure 2b). Once again a discontinuity appears between the regions of energy pumping and no energy pumping. Due to this high sensitivity to design and excitation perturbations, techniques for the design optimization of NESs must be tailored to stay away from the inefficient regions (non energy pumping as well as low $E_{NES_{inf}}$ values).

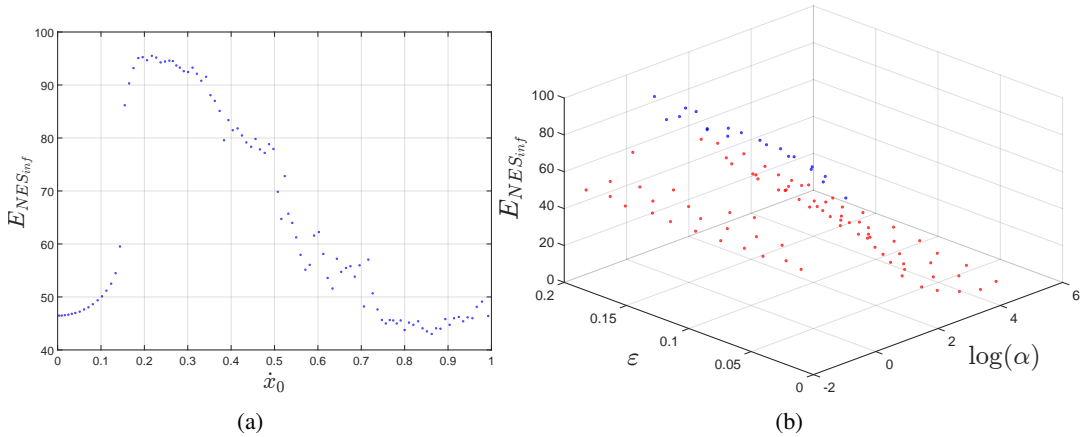


Figure 2: Discontinuities in $E_{NES_{inf}}$ metric. (a) $E_{NES_{inf}}$ response to variations in \dot{x}_0 , with $\varepsilon=0.1$, $\alpha=1$, $\lambda_1=0.004$, $\lambda_2=0.008$, $\omega_1=1$. (b) $E_{NES_{inf}}$ response to variations in α and ε , $\lambda_1=0.01$, $\lambda_2=0.01$, $\omega_1=5$ and $\dot{x}_0=5$ with clustering on $E_{NES_{inf}}$ values.

6. Identification of failure regions

6.1. Clustering

The first step in reliability based design optimization is to segregate efficient and inefficient NES behaviors. The discontinuity illustrated in the previous section enables such a classification, however the location of the discontinuities is often difficult to obtain, especially in high dimensional space. For this reason, a clustering technique such as K-means constructed from a design of experiments can be used without any *a priori* knowledge

of the location of the discontinuities. However, the clustering technique does not always identify properly the clusters as there can be a wide range of energy values over the design space. In order to help the clustering algorithm, samples corresponding to “low” energy levels are removed. This low level energy is found by setting α to its minimum value while maintaining the other parameters at their mean value. Although this approach is rather heuristic, it was shown for the problems treated to provide a proper clustering. An example of clustering in the ε and α space using the proposed technique is depicted in figure 2b.

6.2. SVM

Beyond clustering of the system’s responses, we would like to identify the region of the parameter space where the efficiency of the NES is “acceptable”. In other words, we would like to find the region of the space corresponding to the cluster of better efficiency, using the $E_{NES_{inf}}$ metric. For this purpose, we will use a technique referred to as explicit design space decomposition (EDSD) [1]. The basic idea is to construct the boundary separating two classes of samples (e.g., belonging to the two clusters) in terms of chosen parameters. This is achieved using a Support Vector Machine (SVM) which provides an explicit expression of the boundary in terms of the parameters. The SVM boundary is trained using a design of experiments.

6.3. Refinement of the SVM boundary. Adaptive sampling.

Because the approximated SVM boundary might not be accurate, an adaptive sampling scheme is used to refine the boundary. The sampling algorithm is described in detail in [1]. A fundamental aspect of the algorithm is the selection of samples in the sparse regions of the space (i.e., as far away as possible from existing samples) and also in the regions of highest probability of misclassification by the SVM. The latter criterion is obtained by locating the samples on the SVM. These samples are found by solving the following global optimization problem (side constraints omitted):

$$\begin{aligned} \max_{\mathbf{x}} \quad & \|\mathbf{x} - \mathbf{x}_{nearest}\| \\ \text{s.t.} \quad & s(\mathbf{x}) = 0 \end{aligned} \quad (4)$$

The results section will provide examples of two and three dimensional boundaries constructed using both design and aleatory variables.

7. Reliability Based Design Optimization

The efficient calculation of probabilities with SVM using Monte-Carlo simulations can be used towards the solution of a reliability-based design optimization (RBDO) problem [5], which in the case of a NES, could be formulated as follows:

$$\begin{aligned} \max_{\mu^d} \quad & \mathbb{E}(E_{NES_{inf}}(\mathbf{X}^d, \mathbf{X}^a)) \\ \text{s.t.} \quad & \mathbb{P}((\mathbf{X}^d, \mathbf{X}^a) \in \Omega) \leq P_f \\ & \mu_{\min}^d \leq \mu^d \leq \mu_{\max}^d \end{aligned} \quad (5)$$

where \mathbb{E} is the expected value, μ^d is the vector of means of the distributions of the random design variables \mathbf{X}^d . \mathbf{X}^a are aleatory random variables which contribute to the expected value of the objective function as well as the probabilistic constraints, but whose hyper-parameters are not to be optimized. Ω is the failure region as defined by the SVM boundary, P_f is a target probability.

Note that the probabilistic constraint in the previous problem cannot be used as such because of the noise introduced by the Monte-Carlo simulations which would make the constraint non-differentiable. For this reason, this constraint is typically approximated using a response surface or a metamodel such as Kriging. To regularize the problem further, the reliability index β is approximated instead of the probability P_f itself [5]. β can be defined using the standard cumulative distribution function Φ :

$$\beta = -\Phi^{-1}(P_f) \quad (6)$$

To further reduce computational time and make this RBDO problem tractable, the objective function (i.e., the expected value) as well as the energy are both approximated using a Kriging metamodel.

8. Results

The first two RBDO problems solved use NES parameters as random design variables and main system initial velocity \dot{x}_0 as an aleatory variable. The parameters of the main system (ω_1 , and λ_1) are fixed. In the first problem, only α and ε are random design variables while λ_2 is fixed. In the second problem all three NES design parameters are random design variables. These problems focus on optimally tuning a NES for a given main system so that the expected value of the efficiency is maximized for a range of initial main system velocities. In both cases the failure

domain Ω is defined by the SVM constructed using the clustering technique described in Section 6.1. In all cases 10^6 Monte-Carlo samples are used.

8.1. 1 NES. 3D RBDO with α, \dot{x}_0 , and ε

$$\begin{aligned} \max_{\mu_\alpha, \mu_\varepsilon} \quad & \mathbb{E}(E_{NES_{inf}}(\mu_\alpha, \mu_\varepsilon, \dot{x}_0)) \\ \text{s.t.} \quad & \mathbb{P}((\alpha, \varepsilon, \dot{x}_0) \in \Omega) \leq 0.15 \\ & -2 \leq \log(\mu_\alpha) \leq 5 \\ & 0.01 \leq \mu_\varepsilon \leq 0.2 \qquad 1 \leq \dot{x}_0 \leq 10 \end{aligned} \tag{7}$$

where $\log(\alpha)$ and ε follow normal distributions: $\log(\alpha) \sim N(\mu_{\log(\alpha)}, 0.07^2)$ and $\varepsilon \sim N(\mu_\varepsilon, 0.0019^2)$. The standard deviations correspond to 1% of the range of $\log(\alpha)$ and ε respectively. The excitation follows a uniform distribution $\dot{x}_0 \sim U(1, 10)$. The fixed parameters are $\lambda_1 = \lambda_2 = 0.01$ and $\omega_1 = 5$.

The failure region Ω (i.e., the SVM) is presented in Figure 3. The Kriging approximations $\tilde{\mathbb{E}}(\tilde{E}_{NES_{inf}})$ and β as well as the training points are depicted in Figures 4a and 4b. It is noteworthy that the approximation of the energy is built using the cluster with highest values only. Approximation error metrics are provided in Table 2.

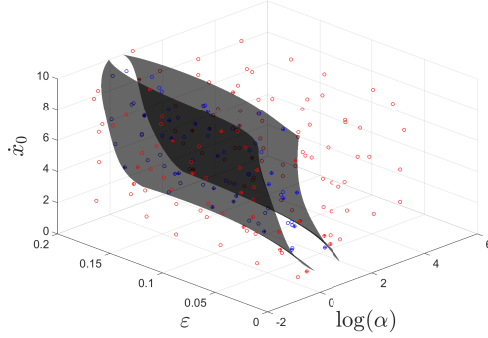


Figure 3: SVM separating the two levels of NES efficiency identified through clustering of $E_{NES_{inf}}$ for α , ε , and \dot{x}_0 .

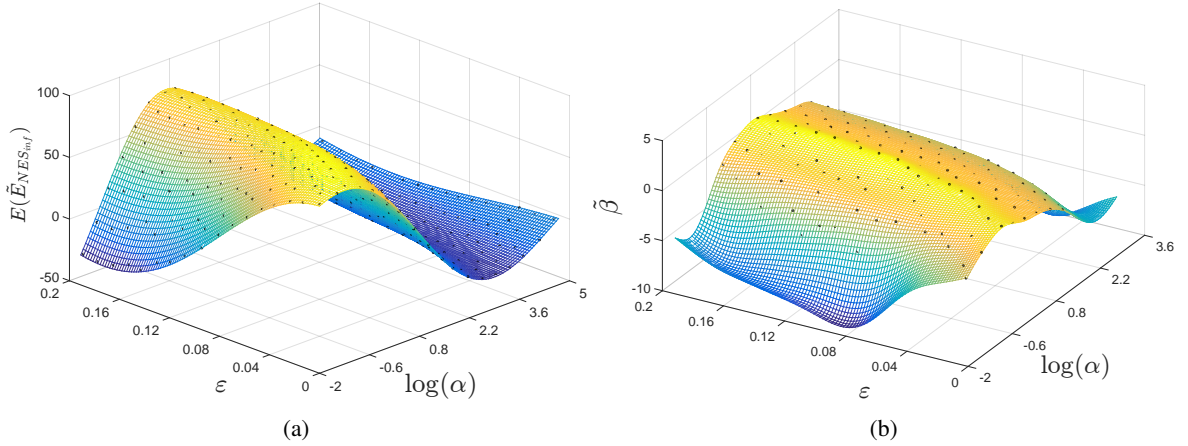


Figure 4: Training and approximations of (a) $\mathbb{E}(\tilde{E}_{NES_{inf}})$ and (b) β for RBDO problem varying α , ε , and \dot{x}_0 .

The RBDO results are given in Figure 5 and summarized in Table 1. The actual probability of failure (as opposed to the approximated one) calculated based on the SVM is also provided in the table.

Table 1: Results table for 1 NES RBDO problem varying α , ε , and \dot{x}_0 .

Probabilistic Optimum	
α	1.32
ε	0.099
P_f from $\tilde{\beta}$	0.15
P_f from SVM	0.19
$\tilde{\mathbb{E}}(\tilde{E}_{NES_{inf}})$	84.9 %
$\mathbb{E}(E_{NES_{inf}})$	77.6 %

Table 2: Error metrics table for 1 NES RBDO problem varying α , ε , and \dot{x}_0 .

Approximation	RMAE	R^2
$\tilde{E}_{NES_{inf}}$	1.11	0.91
$\tilde{\beta}$	0.171	0.99

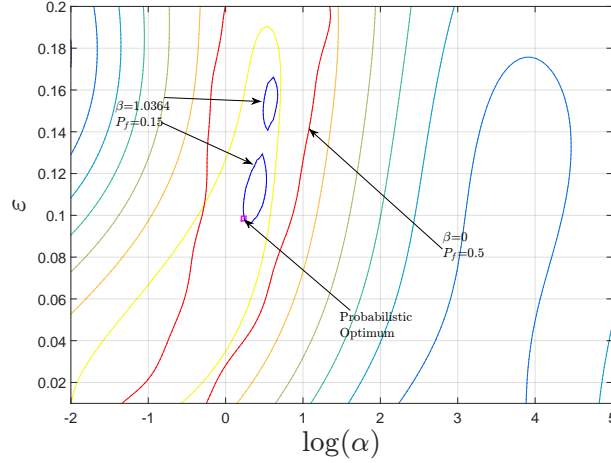


Figure 5: Results plot for 1 NES RBDO problem varying α , ε , and \dot{x}_0 .

8.2. 1 NES 4D RBDO ($\alpha, \dot{x}_0, \lambda_2$, and ε)

This RBDO problem adds λ_2 as a random design variable with a normal distribution. In this problem all three NES parameters are treated as random design variables, while \dot{x}_0 is still treated as an aleatory variable.

$$\begin{aligned}
 & \max_{\mu_\alpha, \mu_\varepsilon, \mu_{\lambda_2}} \mathbb{E}(E_{NES_{inf}}(\mu_\alpha, \mu_\varepsilon, \mu_{\lambda_2}, \dot{x}_0)) & (8) \\
 & s.t. \quad \mathbb{P}((\alpha, \varepsilon, \lambda_2, \dot{x}_0) \in \Omega) \leq 0.2 \\
 & \quad \quad -2 \leq \log(\mu_\alpha) \leq 5 \quad \quad \quad 0.01 \leq \mu_\varepsilon \leq 0.2 \\
 & \quad \quad 0.001 \leq \mu_{\lambda_2} \leq 0.1 \quad \quad \quad 1 \leq \dot{x}_0 \leq 10
 \end{aligned}$$

where $\log(\alpha)$, ε , and λ_2 follow normal distributions: $\log(\alpha) \sim N(\mu_{\log(\alpha)}, 0.07^2)$, $\varepsilon \sim N(\mu_\varepsilon, 0.0019^2)$, and $\lambda_2 \sim N(\mu_{\lambda_2}, 0.00099^2)$.

Error metrics for this four dimensional problem are used to check the quality of the Kriging approximations (Table 4).

Table 3: Results of 1 NES 4D RBDO problem with α , ε , λ_2 , and \dot{x}_0 varied.

Approximation	RMAE	R^2
$\tilde{E}_{NES_{inf}}$	1.61	0.76
$\tilde{\beta}$	1.61	0.97

Table 4: Error metrics of 1 NES 4D RBDO problem with α , ε , λ_2 , and \dot{x}_0 varied.

Probabilistic Optimum	
α	2.76
ε	0.16
λ_2	0.09
P_f from $\tilde{\beta}$	0.00
P_f from SVM	0.00
$\tilde{\mathbb{E}}(\tilde{E}_{NES_{inf}})$	95.7 %
$\mathbb{E}(E_{NES_{inf}})$	96.1 %

8.3. 2 NES RBDO (α_1, α_2 , and \dot{x}_0). Comparison to 1 NES.

The final RBDO problem demonstrates the efficiency of a two NES system as compared to a single NES system. For the single NES problem, the nonlinear stiffness α of the NES and the initial velocity \dot{x}_0 are varied and the corresponding optimization problem is:

$$\begin{aligned} \max_{\mu_\alpha} \quad & \mathbb{E}(E_{NES_{inf}}(\mu_\alpha, \dot{x}_0)) \\ \text{s.t.} \quad & \mathbb{P}((\alpha, \dot{x}_0) \in \Omega) \leq 10^{-3} \\ & -2 \leq \log(\mu_\alpha) \leq 5 \quad 1 \leq \dot{x}_0 \leq 10 \end{aligned} \quad (9)$$

where $\log(\alpha)$ follows a normal distribution: $\log(\alpha) \sim N(\mu_{\log(\alpha)}, 0.21^2)$. The standard deviations correspond to 3% of the range of $\log(\alpha)$. $\dot{x}_0 \sim U(1, 10)$ and $\lambda_1 = \lambda_2 = 0.01$, $\varepsilon = 0.1$, and $\omega_1 = 5$. The two dimensional SVM is given in Figure 7a. The problem does not have a feasible solution with one NES. In fact, the minimum probability of failure is over 20%. The approximated $\tilde{\mathbb{E}}(\tilde{E}_{NES_{inf}})$ value at this point is 82.4%. The error metrics for the Kriging fits for this problem are given in table 5.

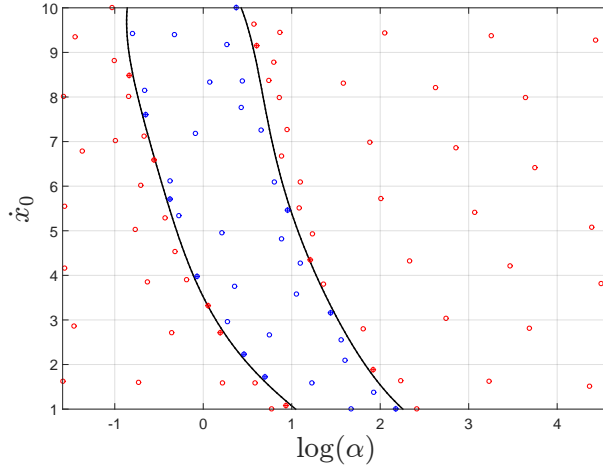


Figure 6: SVM for 1 NES problem varying α and \dot{x}_0 .

Table 5: One NES problem error metrics.

Approximation	RMAE	R^2
$\tilde{E}_{NES_{inf}}$	0.42	0.96
β	0.047	0.99

For the 2 NES case, the optimization problem becomes:

$$\begin{aligned} \max_{\mu_{\alpha_1}, \mu_{\alpha_2}} \quad & \mathbb{E}(E_{NES_{inf}}(\mu_{\alpha_1}, \mu_{\alpha_2}, \dot{x}_0)) \\ \text{s.t.} \quad & \mathbb{P}((\alpha_1, \alpha_2, \dot{x}_0) \in \Omega) \leq 10^{-3} \\ & -2 \leq \log(\mu_{\alpha_1}) \leq 5 \quad -2 \leq \log(\mu_{\alpha_2}) \leq 5 \quad 1 \leq \dot{x}_0 \leq 10 \end{aligned} \quad (10)$$

where $\log(\alpha_1)$ and $\log(\alpha_2)$ follow normal distributions: $\log(\alpha_1) \sim N(\mu_{\log(\alpha_1)}, 0.21^2)$ $\log(\alpha_2) \sim N(\mu_{\log(\alpha_2)}, 0.21^2)$. The standard deviations correspond to 3% of the range of $\log(\alpha)$, $\dot{x}_0 \sim U(1, 10)$, $\lambda_1 = \lambda_2 = 0.01$, and $\omega_1 = 5$. In addition, the mass of each NES is 5% (i.e., $\varepsilon_1 = \varepsilon_2 = 0.05$) of the main system total mass, adding to a total NES mass of 10%, which is the value used in the one NES problem. The three dimensional SVM approximation of the failure domain is depicted in Figure 7a. The SVM appears symmetric because the fixed NES parameters are identical for the two NESs. The approximation $\tilde{\mathbb{E}}(\tilde{E}_{NES_{inf}})$ and the training points are given in figure 7b. The error metrics for all Kriging approximations are given in Table 7. The β approximation is given in Figure 8a. Finally, the RBDO results are given in Figure 8b and Table 6. The actual value of the probability of failure as calculated from the SVM is given in Table 6.

The two NES system gives a more robust optimum, successfully achieving a probability of failure of 10^{-3} . The $\mathbb{E}(\tilde{E}_{NES_{inf}})$ value is also larger in the two NES case. The distributions of $E_{NES_{inf}}$ over the \dot{x}_0 space for the optimal

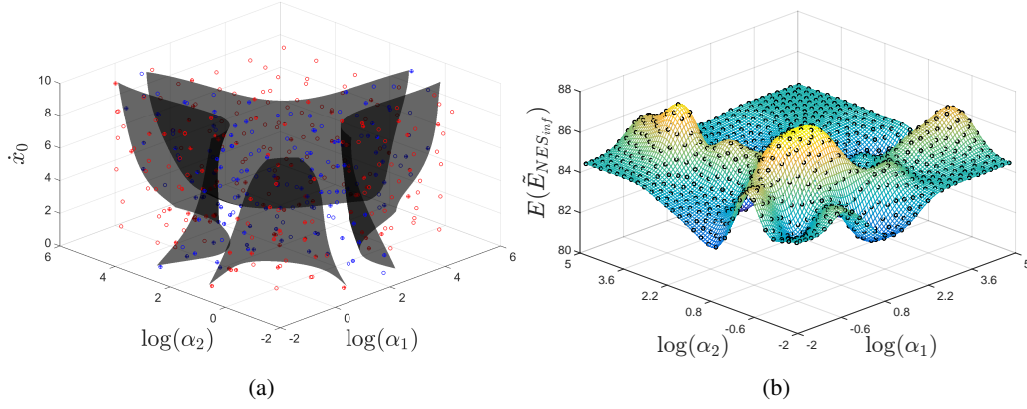


Figure 7: (a) Three dimensional SVM and (b) $\mathbb{E}(\tilde{E}_{NES_{mf}})$ approximation for two NES RBDO varying α_1 , α_2 , and \dot{x}_0 .

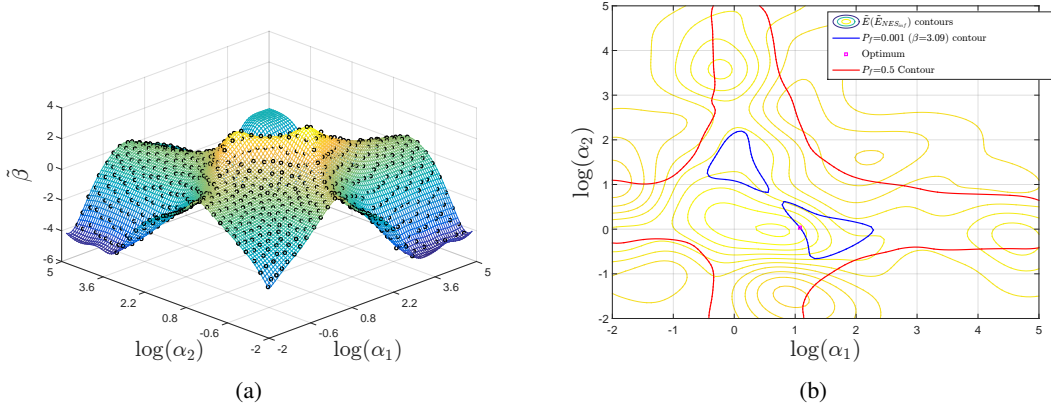


Figure 8: (a) β approximation and (b) RBDO results for two NES RBDO varying α_1 , α_2 , and \dot{x}_0

Table 6: Results table for 2 NES RBDO problem varying α_1 , α_2 , and \dot{x}_0 .

	Probabilistic Optimum
α_1	11.9
α_2	1.08
P_f from $\tilde{\beta}$	$1.00 * 10^{-3}$
P_f from SVM	$9.0 * 10^{-4}$
$\mathbb{E}(\tilde{E}_{NES_{mf}})$	90.3 %
$\mathbb{E}(E_{NES_{mf}})$	90.6 %

Table 7: Error metrics table for 2 NES RBDO problem varying α_1 , α_2 , and \dot{x}_0 .

Approximation	RMAE	R^2
$\tilde{E}_{NES_{mf}}$	0.00	0.99
$\tilde{\beta}$	0.080	0.99

NESs are given in figure 9. The two NES system has a higher $E_{NES_{mf}}$ value for most of the excitation range. The two NES system is more robust and the decline in $E_{NES_{mf}}$ is slower as \dot{x}_0 increases.

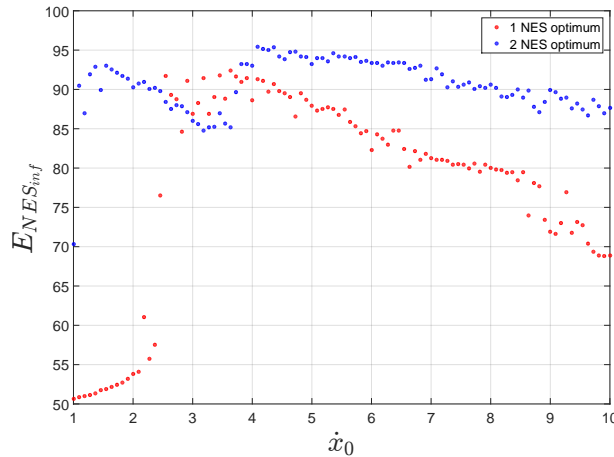


Figure 9: Variation of $E_{NES_{inf}}$ with respect to \dot{x}_0 for the optima found through RBDO of one and two NESs varying α and \dot{x}_0 .

9. Conclusion

This paper introduces a new methodology for the optimization under uncertainty of a Configuration II NES. The methodology stems from the realization that the efficiency of a NES might be discontinuous and highly sensitive to uncertainty. For this reason, specific tools such as SVM and clustering are used to perform the optimization and propagate uncertainty. In addition a one NES and a two NES system were compared. The two NES system is more robust and gives a higher expected performance than the one NES system with an equal total NES mass. The next steps of this research will continue to increase the dimensionality for both the single NES and the multi NES systems. A transition towards more realistic simulations will be explored, particularly through the use of finite element modeling.

10. References

- [1] A. Basudhar and S. Missoum. An improved adaptive sampling scheme for the construction of explicit boundaries. *Structural and Multidisciplinary Optimization*, pages 1–13, 2010.
- [2] E. Boroson, S. Missoum, P.-O. Mattei, and C. Vergez. Optimization under uncertainty of nonlinear energy sinks. In *ASME 2014 International Design Engineering Technical Conferences and Computers and Information in Engineering Conference*. American Society of Mechanical Engineers, 2014.
- [3] O. Gendelman, L. Manevitch, A. F. Vakakis, and R. M’closkey. Energy pumping in nonlinear mechanical oscillators: Part i: Dynamics of the underlying hamiltonian systems. *Journal of Applied Mechanics*, 68(1):34–41, 2001.
- [4] Y. S. Lee, A. F. Vakakis, L. A. Bergman, D. M. McFarland, and G. Kerschen. Enhancing the robustness of aeroelastic instability suppression using multi-degree-of-freedom nonlinear energy sinks. *AIAA journal*, 46(6):1371–1394, 2008.
- [5] S. Missoum, C. Dribusch, and P. Beran. Reliability-based design optimization of nonlinear aeroelasticity problems. *Journal of Aircraft*, 47(3):992–998, 2010.
- [6] T. A. Nguyen and S. Pernot. Design criteria for optimally tuned nonlinear energy sinkspart 1: transient regime. *Nonlinear Dynamics*, 69(1-2):1–19, 2012.
- [7] A. F. Vakakis. *Nonlinear targeted energy transfer in mechanical and structural systems*, volume 156. Springer Science & Business Media, 2008.
- [8] A. F. Vakakis, A. N. Kounadis, and I. G. Raftoyiannis. Use of non-linear localization for isolating structures from earthquake-induced motions. *Earthquake engineering & structural dynamics*, 28(1):21–36, 1999.
- [9] N. Wierschem, B. Spencer Jr, L. Bergman, and A. Vakakis. Numerical study of nonlinear energy sinks for seismic response reduction. In *Proceedings of the 6th International Workshop on Advanced Smart Materials and Smart Structures Technology (ANCRiSST 2011)*, pages 25–26, 2011.